



Response of green synthesized drug blended silver nanoparticles against periodontal disease triggering pathogenic microbiota

Neeraj Kumar Fuloria^{1*}, Shivkanya Fuloria¹, Kok Yik Chia¹, Sundram Karupiah¹, Kathiresan Sathasivam²

¹Pharmaceutical Chemistry Unit, Faculty of Pharmacy, AIMST University, Kedah, Malaysia

²Department of Biotechnology, Faculty of Applied Sciences, AIMST University, Kedah, Malaysia

ARTICLE INFO

Article history:

Received on: November 28, 2018

Accepted on: February 28, 2019

Available online: July 04, 2019

Key words:

Nanocomposites, microbiota, periodontitis, antibacterial, *Erythrina fusca*, optimization

ABSTRACT

Objective: Evidences for microorganisms to predominate periodontal disease, alteration of human pathogen shifted microbiota by *Erythrina fusca*, and antimicrobial response potentiation by ecofriendly silver nanoparticles (AgNPs) intended present study to perform green synthesis of AgNPs and evaluate against periodontal disease triggering pathogenic microbiota.

Material and Methods: Present study involved green synthesis of AgNPs using *Erythrina fusca* leaves aqueous extract (EFLAE), followed by optimization, characterization, stability, and evaluation of antimicrobial potential of biosynthetic AgNPs against periodontitis causing pathogenic human microflora (*Pseudomonas aeruginosa*, *Escherichia coli*, *Streptococcus pyogenes*, and *Staphylococcus aureus*).

Results: The AgNPs green synthesis success was based on brown coloration and surface plasmon resonance signal at 433 nm. UV-Visible spectrometry driven optimization determined 5 mM AgNO₃ concentration, 1:9 EFLAE and AgNO₃ volumetric ratio, pH 7, 60°C temperature, and 2 hours' time as parametric requirements for AgNPs biosynthesis. Stability studies revealed signal appearance between 415 and 424 nm supporting AgNPs stability. Characterization studies recognized shifted and broadened Fourier transformed infrared bands of AgNPs revealing silver capping by biochemical moieties of EFLAE; AgNPs size below 32 nm in field emission scanning electron microscopic micrograph; X-ray diffraction signals at 38.95, 44.97, 64.92, and 78.97 representing 111, 200, 220, and 311 AgNPs silver cubic structure planes; and elemental silver 83.66%, carbon 11.87%, and oxygen 4.47% in energy-dispersive X-ray spectrum. Optimized and characterized biogenic AgNPs, when evaluated against periodontal disease-causing pathogenic microflora using well diffusion method, exhibited maximum inhibitory zone (in mm) against *Bacillus cereus* (13 and 18), followed by *P. aeruginosa* (11 and 19), *E. coli* (10 and 18), and *S. pyogenes* (9 and 15) in 50 and 100 µg/ml administered dose.

Conclusion: Present study concludes that biogenic AgNPs synthesized using EFLAE possess high inhibition potential against periodontitis triggering pathogens (*E. coli*, *B. cereus*, *S. pyogenes*, and *P. aeruginosa*) of microbiota, and recommends EFLAE as potential source for AgNPs green synthesis.

1. INTRODUCTION

Research studies in recent years advocate human microbiota to possess 1:1 ratio of human cells and bacteria [1,2]. Disturbance in such ratio of microflora leads to several infections, diseases, and wide range of inflammatory diseases [3]. Among inflammatory diseases, the periodontitis is considered as most complex polymicrobial inflammatory disorder. Periodontitis is associated with dysbiosis of dental biofilm which manifests in chronic inflammation of periodontal lining tissues. This results in damage

of alveolar bone and subsequent tooth destruction [4]. Pathogenic microbiota and chronic inflammation in periodontitis contribute in progression and onset of many other systemic diseases, such as cardiovascular diseases [5,6], metabolic syndrome [7], diabetes [8], rheumatoid arthritis [9], respiratory disease [10], chronic kidney disease [11], obesity [12], and cancer [13]. Therefore, shift in content of oral microflora is considered as primary factor that contributes to periodontitis [14]. Studies witness that disturbance of microbiota may activate *P. aeruginosa*, *E. coli*, *S. pyogenes*, and *B. cereus* [15–17]. There is high occurrence of *P. aeruginosa*, *E. coli*, *S. pyogenes*, and *B. cereus* in periodontal site of chronic patients of periodontitis [18]. Studies consider periodontal disease as the most oral infectious disease that is predominated by microorganism [19].

*Corresponding Author

Neeraj Kumar Fuloria, Faculty of Pharmacy, AIMST University, Kedah, Malaysia. E-mail: nfuloria@gmail.com

Manifestation of multiple drug resistance, prolonged treatment, and increased risk for mortality attributed to extensive use of conventional antimicrobial agents have geared up the nanocomposites research in current decade [20–22]. As a result, recent decade recorded mettlesome development in the field of metal nanocomposites with profound application in microelectronics, photonics, and medicines [23,24]. Among metallic nanoparticles, the high potential of silver nanoparticles (AgNPs) to enhance the antimicrobials and other biomedicine activity always motivate the investigators [25–29]. The AgNPs are reported as powerful tools against multiple drug-resistant bacteria, such as *E. coli*, erythromycin-resistant *S. pyogenes*, *P. aeruginosa*, and *B. cereus* [30,31]. Investigations assert several methods for metal nanocomposites synthesis like microwave irradiation [32], heat evaporation [33], chemical reduction [34], and electrochemical reduction [35]. The AgNPs synthesis using asserted methods mandates the use of surface passivators to prevent agglomeration. The use of passivators such as thiophenol, mercaptoacetate, and thiourea in synthesis of AgNPs may result in environmental pollution [36]. The AgNPs synthesis by chemical method may lead to toxic entities adsorption over particles surface and manifest many adverse effects during application. Though AgNPs can be formulated by several methods, but the method that offers non-toxicity, high yield, high economy, and environmental safety is a major concern [37]. Nanocomposite synthesis using plant materials is considered as green, as it does not involve hazardous chemicals. The benefits of environmental friendliness, simplicity, cost-effectiveness, stability, and reproducibility, attached with the biogenic synthesis justify the importance of green synthesis of AgNPs [37,38]. Studies suggest alteration of human gut bacteria by addition of certain vegetables into controlled vegetable diet [39]. The traditional herb *Erythrina fusca* commonly eaten as vegetable is known to possess alkaloid, glycoside, saponin, tannin, triterpenoid, and steroid as chief constituents. The high efficacy of *E. Fusca* in periodontitis always draws investigators attention [19].

Based on the literary research evidences, it was hypothesized that blending of highly efficacious drug *E. Fusca* into AgNPs would offer a synergistic remedy to combat pathogenic microbiota triggered periodontal disease. Hence, based on complex disorders of periodontitis and expected benefits attached with blend of AgNPs and *E. fusca*, the present study was intended to perform the green synthesis of AgNPs using *Erythrina fusca* leaves aqueous extract (EFLAE), followed by biogenic AgNP's optimization, stability, characterization, and evaluation against common pathogenic human microbiota (*P. aeruginosa*, *B. cereus*, *S. pyogenes*, and *E. coli*) that triggers periodontal disease.

2. MATERIALS AND METHODS

2.1. Selection of Material

The AgNPs were biosynthesized using EFLAE. The major chemicals, such as silver nitrate, dimethyl sulfoxide, sodium hydroxide (NaOH), potassium bromide (KBr), and Muller Hilton agar were acquired from Sigma Aldrich, SD Fine, Fisher chemicals, and Hi-Media. Prior to antibacterial activity, the glasswares were washed with deionized water, and followed by drying for 2 hours at 160°C (whereas plastic wares were autoclaved).

2.2. Preparation of *Erythrina fusca* Leaves Aqueous Extract

Fresh leaves of *E. fusca* free of decay or mold were collected from the province of Sungai Petani, Kedah state, Malaysia and washed with fast flowing tap water (to remove the dust particles). The leaves were air dried, cut into small pieces using scissor (sterilized using 70% ethanol), placed into a beaker containing 500 ml of distilled water, and finally, blended into fine pieces using a blender. The blend was heated until 100°C and brought down to room temperature. The mixture was filtered using double muslin cloth and a filter paper (Whatman No. 1). The obtained EFLAE was stored at 4°C in refrigerator for further use in biosynthesis of for further synthesis of AgNPs. The experimental protocol was based on reported method with slight modifications [40].

2.3. Green Synthesis of AgNPs

The green synthesis of AgNPs involved addition of 9 ml, 5 mM silver nitrate solution (prepared by dissolving 0.425 g of AgNO₃ in 500 ml of deionized water) into 10 ml volumetric flask containing 1 ml of fresh EFLAE. The mixture was stirred for 2 minutes and kept at 60°C for 2 hours to undergo reduction. After the confirmation of AgNO₃ reduction (based on a color change to brown), the resultant solution was centrifuged at 3,000 rpm for 10 minutes (to separate the AgNPs). The supernatant layer was discarded to offer crude AgNPs. Crude AgNPs were collected, rewashed, and centrifuged. The washing and centrifugation processes were repeated two to three times using deionized water to remove any substances on the surface of the AgNPs, and finally, air dried to yield pure AgNPs. The AgNPs synthesis was based on standard reference procedure with slight modification [41–43].

2.3.1. UV-Visible analysis

The biogenic AgNPs synthesis success was confirmed by UV-Visible spectral analysis. After dilution of small aliquot of biosynthesized AgNPs in deionized water (1 ml test sample with 4 ml deionized water), the test mixture was subjected to UV-Visible spectral analysis at room temperature to observe surface plasmon resonance (SPR) signal. The analysis was done at 400–800 nm using Shimadzu U-2800 spectrophotometer with a scanning speed of 300 nm/minute. The monitoring of generated UV-Visible absorption spectrum determined reduction of Ag⁺ ions. The AgNP solution exhibited an absorbance signal at 433 nm. The analysis was carried out as per standard reference procedure with minor modifications [41–43].

2.4. AgNPs Biosynthesis Optimization Study

The green synthesis of AgNPs was optimized by determining the optimum concentration of AgNO₃, volumetric ratio of EFLAE to AgNO₃, pH, temperature, and time required for the green synthesis of AgNPs. The optimization methodology was followed according to the reported procedure with minor modifications [43–47].

2.4.1. Optimization of concentration of AgNO₃ and volumetric ratio of EFLAE to AgNO₃

According to the method given for green synthesis of AgNPs in present study, 18 individual reaction mixtures were prepared

and maintained in same conditions, except for volumetric ratio of EFLAE to AgNO₃ and concentration of AgNO₃. The reaction mixtures were prepared in three volumetric ratios of EFLAE to AgNO₃ (1:9, 2:8 and 5:5). For each of the three volumetric ratios, six different concentrations of AgNO₃ were taken (0.25, 0.50, 0.75, 1, 2, and 5 mM). Each of the 18 reaction mixtures were subjected to visual examination (to monitor color change from yellow to brown) and UV-Visible spectrometric analysis (to observe SPR signal in UV-Visible spectrum) to determine the ideal concentration of AgNO₃ and best volumetric ratio of EFLAE to AgNO₃ required for green synthesis of pure AgNPs.

2.4.2. Optimization of pH

Following the same experimental protocol given for green synthesis of AgNPs in present study, the three individual solution mixtures were prepared and maintained in same conditions, except for pH. Three solution mixtures were maintained each at different pH (4, 7, and 8). The pH of solution mixture was adjusted by addition of 0.1 N HCl and 0.1 N NaOH. Each of the three solution mixtures with different pH was subjected to visual examination (to observe change in color from yellow to brown) and UV-Visible analysis (to observe SPR peak) to determine the ideal pH required for production of pure biogenic AgNPs.

2.4.3. Optimization of temperature

As per the experimental procedure mentioned for green synthesis of AgNPs in present study, the three individual reaction mixtures were prepared and maintained in same conditions, except for temperature. The three reaction mixtures were maintained each at three different temperatures (8°C–10°C, 25°C room temperature, and 60°C). Each of the three solution mixtures with different temperatures was subjected to visual examination (to observe color change from yellow to brown) and UV-Visible analysis (for monitoring SPR signal) to determine the suitable temperature required for green synthesis of pure AgNPs.

2.4.4. Optimization of time

According to the experimental method given for green synthesis of AgNPs in present study, the solution mixture was prepared and maintained with the same conditions, except for time. The solution mixture was monitored for completion of reaction at different time intervals that is ½ hour, 1 hour, 2 hours, and 4 hours. After the stated time intervals, the solution mixture was subjected to visual examination (for change in color from yellow to brown) and UV-Visible spectrometric analysis (for observation of SPR signal) to determine the ideal time required for biosynthesis of pure AgNPs.

2.5. AgNPs Stability Study

After optimization of all key parameters for green synthesis of AgNPs, the yielded pure biogenic AgNPs were subjected to stability studies. The stability of biogenic AgNPs was assessed based on location of SPR signal (in range of 340–540 nm) in the UV-Visible absorption spectrum recorded by UV-Visible spectrophotometer. The measurements were made after every ½ hour, 2 hours, 1 day, 7 day, 15 days, and 30 days. The experimental

procedure was performed based on reported studies with slight modifications [42–44].

2.6. AgNPs Characterization Study

After optimization and stability studies, the biogenic AgNPs were subjected to characterization studies using several techniques mentioned in the literature [47–50]. Before commencement of characterization studies, the AgNPs were repeatedly washed and centrifuged using deionized water. This process was done to avoid the chances of interference of unbound residual biochemical entities of EFLAE with Fourier transformed infrared (FTIR), field emission scanning electron microscopic (FESEM), X-ray diffraction (XRD), and energy-dispersive X-ray (EDX) data of AgNPs biosynthesized from EFLAE. The successful formation of AgNPs was confirmed by UV-Visible spectral analysis using Shimadzu U-2800 spectrophotometer and FTIR spectrometric analysis using PerkinElmer SLE/MS4/29 instrument. The AgNPs mean particle diameter was determined by FESEM analysis using FEI Nova NanoSEM 450 instrument. The biogenic AgNPs morphology was determined based on XRD data. The XRD pattern was recorded using PANalytical X'Pert PRO MRD PW 3040/60 X-ray diffractometer, operated at 40 kV and 40 mA, and using CuKαβ radiation with wavelength of Å in the 1.54060 2θ range of 10°C–80°C. The elemental composition of AgNPs was investigated by EDX analysis using FEI Nova NanoSEM 450 with EDX unit.

2.7. AgNPs Antimicrobial Screening Against Pathogenic Microbiota

The biogenic AgNPs were assessed for antimicrobial potential using well diffusion method against *E. coli* (ATCC 10799), *S. pyogenes* (ATCC 19615), *P. aeruginosa* (ATCC 10145), and *B. cereus* (ATCC 11774). The pure and fresh bacterial strain cultures (10⁵–10⁶ CFU/ml) were subcultured on Muller–Hinton (MH) broth at 37°C (beforehand shaken at 200 rpm using rotary shaker). Using a sterile cotton swab, each bacterial culture strain was uniformly swabbed over individual MH agar plates. In each MH plate, wells of 6 mm diameter size were created using a sterile gel puncture. To individual wells of each agar plate, AgNPs were added using a micropipette (50 and 100 µg/ml), EFLAE (50 and 100 µg/ml), and ciprofloxacin (10 µg/ml) each in a volume of 50 µl. Finally, after incubation of plates at 37°C for 24 hours, the zone of inhibition was measured. The experimental protocol was based on reported method with slight modifications [48].

3. RESULTS

3.1. Green Synthesis of AgNPs

The results of green synthesis of AgNPs were based on the visual examination and UV-Visible spectrometric analysis of AgNPs. The AgNO₃ and EFLAE reaction mixture was maintained at 60°C for 2 hours to monitor the color change. After 2 hours, a color change was observed from yellow to brown (Fig. 1). The brown colored solution on UV-Visible spectrometric analysis exhibited a signal at 433 nm (Fig. 2), indicating formation of AgNPs. In Figure 2, curve 1 displayed no AgNPs signal but a signal at 667

nm was observed for EFLAE. The color change was determined as the end point of AgNPs biosynthetic reaction, which indicated formation of AgNPs. The results obtained in present study were based on their presence of SPR signal within the range of results claimed by other standard research [40–45].

3.2. Optimization of Parameters for AgNPs

The green synthesis of AgNPs was optimized using different parameters, such as silver nitrate concentration, the ratio of EFLAE to silver, pH, temperature, and time. The optimization results of present study were verified based on their presence of SPR signal within the range of results claimed by other standard research [41–46].

The UV-Visible spectrometric study over green synthesis of AgNPs based on collective optimization of concentration of AgNO₃ and ratio of EFLAE to AgNO₃ as parameters offered two UV-Visible spectra (Figs. 3 and 4) each containing nine curves. The UV-Visible spectrum given in Figure 3 displayed no absorption signal for AgNPs in any of the nine curves. In Figure 3, curve 1 represents ratio of EFLAE to AgNO₃ (1:9) and AgNO₃ (0.25 mM); curve 2 represents ratio of EFLAE to AgNO₃ (1:9) and AgNO₃ (0.5 mM); curve 3 represents ratio of EFLAE to AgNO₃ (1:9) and AgNO₃ (0.75 mM); curve 4 represents ratio of EFLAE

to AgNO₃ (2:8) and AgNO₃ (0.25 mM); curve 5 represents ratio of EFLAE to AgNO₃ (2:8) and AgNO₃ (0.5 mM); curve 6 represents ratio of EFLAE to AgNO₃ (2:8) and AgNO₃ (0.75 mM); curve 7 represents ratio of EFLAE to AgNO₃ (5:5) and AgNO₃ (0.25 mM); curve 8 represents ratio of EFLAE to AgNO₃ (5:5) and AgNO₃ (0.5 mM); and curve 9 represents ratio of EFLAE to AgNO₃ (5:5) and AgNO₃ (0.75 mM). The UV-Visible spectrum given in Figure 4 exhibited an absorption signal for AgNPs in curve 3 at 439 nm revealing the completion of green synthesis of AgNPs. In Figure 4, curve 1 represents ratio of EFLAE to AgNO₃ (1:9) and AgNO₃ (1 mM); curve 2 represents ratio of EFLAE to AgNO₃ (1:9) and AgNO₃ (2 mM); curve 3 represents ratio of EFLAE to AgNO₃ (1:9) and AgNO₃ (5 mM); curve 4 represents ratio of EFLAE to AgNO₃ (2:8) and AgNO₃ (1 mM); curve 5 represents ratio of EFLAE to AgNO₃ (2:8) and AgNO₃ (2 mM); curve 6 represents ratio of EFLAE to AgNO₃ (2:8) and AgNO₃ (5 mM); curve 7 represents ratio of EFLAE to AgNO₃ (5:5) and AgNO₃ (1 mM); curve 8 represents ratio of EFLAE to AgNO₃ (5:5) and AgNO₃ (2 mM); and curve 9 represents ratio of EFLAE to AgNO₃ (5:5) and AgNO₃ (5 mM). The optimization results of concentration of AgNO₃ and volumetric ratio of extract and AgNO₃ of present study expressed as absorbance signal were in agreement to other studies results [43,45,46].

The UV-Visible experiment on green synthesis of AgNPs based on optimization of pH (4, 7, and 8) generated a UV-Visible spectrum given in Figure 5, containing three curves 1, 2, and 3. The UV-Visible spectrum given in Figure 5 displayed no absorption signals for AgNPs in curves 1 and 3 (related to pH 4 and 8). Figure 5 displayed an absorption signal for AgNPs in curve 2 (related to pH 7) at 426 nm, indicating the completion of green synthesis of AgNPs. The pH optimization result of present study expressed as absorption signal at 426 nm was in range of other research [41,43,45,46].

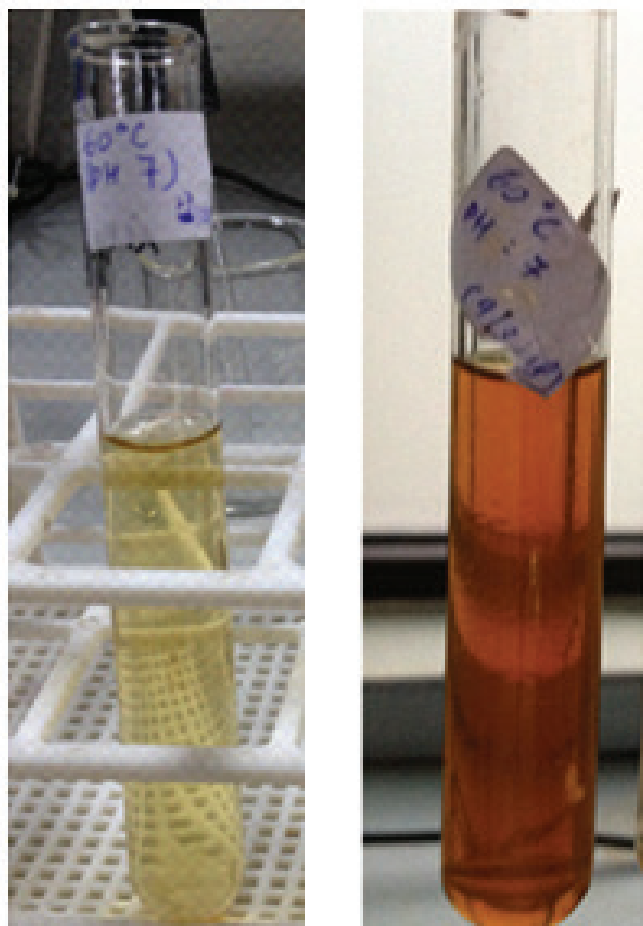


Figure 1: Color change from yellow to brown, indicating formation of AgNPs.

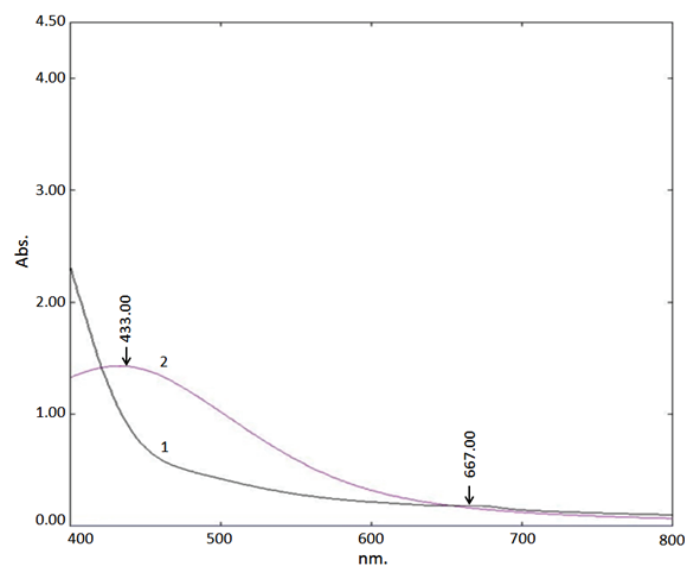


Figure 2: UV-Vis spectrum indicating formation of AgNPs. Presence of SPR signal at 433 nm in curve 2 indicates AgNPs formation, whereas absence of signal in curve 1 of EFLAE represents AgNPs absence.

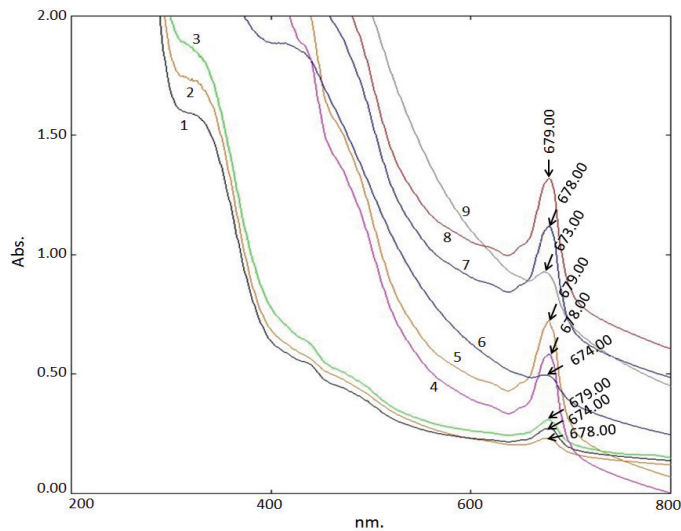


Figure 3: UV-Vis spectrum representing collective optimization of volumetric ratio of EFLAE to AgNO₃, and AgNO₃ molar concentration for AgNPs synthesis. Absence of SPR signal near 400 nm in all nine curves indicates no formation of AgNPs.

The UV-Visible study over green synthesis of AgNPs based on optimization of temperature (8°C–10°C, room temperature, and 60°C) generated a UV-Visible spectrum given in Figure 6, containing three curves 1, 2, and 3. The UV-Visible spectrum given in Figure 6 displayed no absorption signals for AgNPs in curves 1 and 2 (related to 8°C–10°C and room temperature). Figure 6 displayed an absorption signal for AgNPs in curve 3 (related to 60°C) at 412 nm revealing the completion of green synthesis of AgNPs. Resultant data of temperature optimization in present study expressed as absorbance signal were in agreement with the data of other investigations [41,43,45,46].

The UV-Visible analysis over biosynthesis of AgNPs based on optimization of time (½ hour, 1 hour, 2 hours, and 4 hours) generated a UV-Visible spectrum given in Figure 7, containing four curves 1, 2, 3, and 4. The UV-Visible spectrum given in Figure 7 displayed no absorption signals for AgNPs in curve 1 (½ hour) and curve 2 (1 hour). Figure 7 displayed an absorption signal for AgNPs in curve 3 (related to 2 hours) at 412 nm and in curve 4 (related to 4 hours) at 425 nm, indicating the completion of green synthesis of AgNPs. The results of optimization of time, expressed as absorbance signal were in similar results range of other experimental studies [41,43,45,46].

3.3. Stability Study for AgNPs

The UV-Visible spectrometry assisted in the stability study of green synthesized AgNPs. The stability study was conducted for 2 hours, 1 day, 7 days, 15 days, and 30 days (Fig. 8). The Figure 8 displayed 1, 2, 3, 4, and 5 curves for 2 hours, 1 day, 7 days, 15 days, and 30 days, respectively. Figure 8 expressed retention of AgNPs signal in the range of 415–424 nm. The stability results of present study were verified based on their presence of SPR signal within the similar range of results claimed by other standard research [41–43].

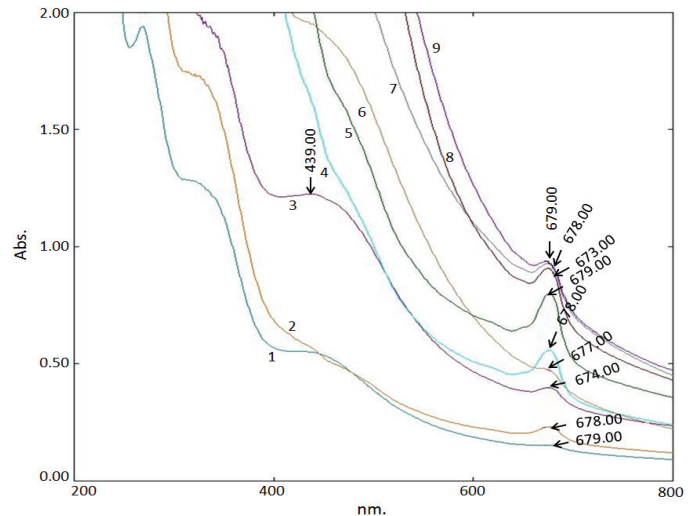


Figure 4: UV-Vis spectrum representing collective optimization of volumetric ratio of EFLAE to AgNO₃, and AgNO₃ molar concentration for AgNPs synthesis. Presence of signal at 439 nm in curve 4 indicates that ratio of EFLAE to AgNO₃ (2:8) and AgNO₃ (1 mM) are optimum for AgNPs biosynthesis.

3.4. Characterization of AgNPs

Prior to characterization, biogenic AgNPs were washed/centrifuged repeatedly with deionized water to avoid interference of their FTIR, FESEM, XRD, and EDX spectra with unbound residual phyto-entities of EFLAE.

3.4.1. Fourier transformed infrared analysis

The FTIR analysis assisted in determination of reduction of Ag⁺ to Ag⁰ and formation of AgNPs. The EFLAE pure FTIR spectrum given in Figure 9 exhibited various bands at 3,415 cm⁻¹ (O-H vibrations), 2,945 cm⁻¹ and 2,884 cm⁻¹ (C-H vibrations), 1,765 and 1,716 cm⁻¹ (C=O vibrations), 1,559 cm⁻¹ (C=N vibrations), and 1,488 and 1,465 cm⁻¹ (C=C vibrations). The FTIR spectrum for AgNPs given in Figure 10 displayed shifted bands 3,420 cm⁻¹ (O-H vibrations), 2,926 and 2,865 cm⁻¹ (C-H vibrations), 1,765 and 1,715 cm⁻¹ (C=O vibrations), 1,553 cm⁻¹ (C=N vibrations), and 1,486 and 1,488 cm⁻¹ (C=C vibrations). The FTIR characterization data results indicated reduction of Ag⁺ to Ag⁰ and formation of AgNPs [47]. The resultant shifting and broadening of absorption bands in FTIR spectrum of AgNPs in comparison to pure extract was supported by other investigations also [45–47].

3.4.2. Field emission scanning electron microscope analysis

The FESEM study was used to determine the size and shape of biogenic AgNPs [49,50]. The FESEM study over biogenic AgNPs resulted in FESEM micrographs given in Figure 11, determined that biosynthesized AgNPs were well dispersed, spherical shaped, and ranged less than 32 nm in size. Similar results were reported in other research over phyto-synthesized AgNPs [49].

3.4.3. X-ray diffraction analysis

The AgNPs synthesized in present study were characterized using powder XRD to confirm the particles as silver and to understand

their structural information. XRD spectrum given in Figure 12 shows the pattern of AgNPs. The XRD spectrum given in Figure 12 exhibited distinctive peaks at 2θ values of 38.07, 45.22, 64.52, and 78.85 corresponding to the 111, 200, 220, and 311 reflection planes, respectively. The XRD pattern results of present study were verified based on agreement with other standard research [49,50].

3.4.4. Energy dispersive X-ray diffraction analysis

The EDX analysis of AgNPs given in Figure 13 exhibited silver (84.63%) as a major constituent element, followed by carbon (11.48%), oxygen (2.36%), and nitrogen (1.53%). Generally, metallic AgNP shows their typical optical absorption peak

approximately at 3 KeV. The EDX analysis results of present study were also verified by matching with other research studies [50].

3.5. Well Diffusion Antimicrobial Activity Against Periodontal Disease Triggering Microbiota

The optimized and characterized green AgNPs were evaluated for their antimicrobial potential against periodontal disease triggering pathogenic human microflora, namely: *P. aeruginosa*, *E. coli*, *S. pyogenes*, and *S. aureus* (resultant data are given in Table 1). As per the data given in Table 1, the biogenic AgNPs, when evaluated against periodontitis causing pathogenic microflora using well diffusion method, exhibited maximum inhibitory zone against *B. cereus* (13 and 18 mm), followed by *P. aeruginosa* (11 and 19 mm),

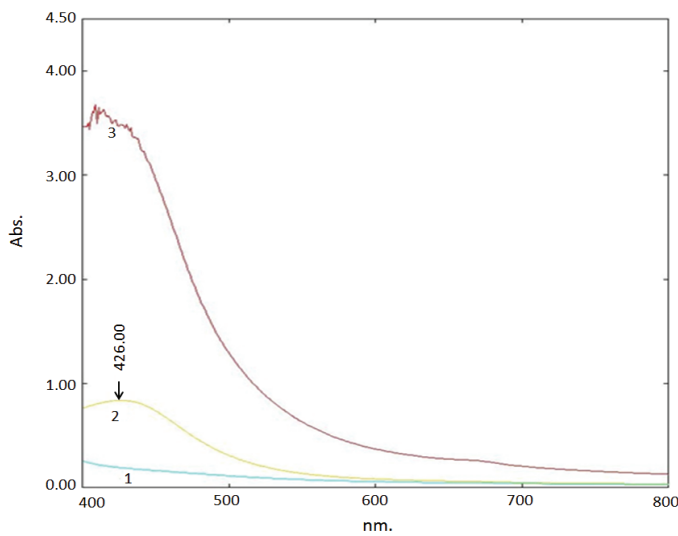


Figure 5: UV-Vis spectrum indicating optimization of pH to synthesize AgNPs. Presence of SPR signal at 426 nm in curve 2 indicates that pH 7 is optimum for AgNPs biosynthesis.

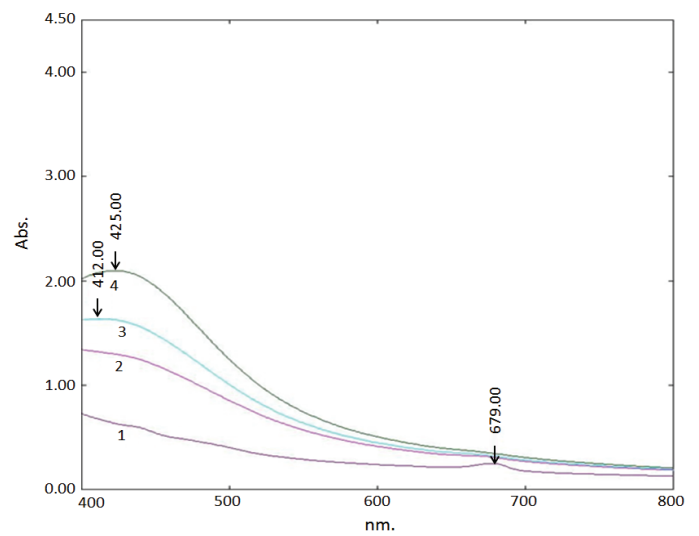


Figure 7: UV-Vis spectrum indicating optimization of time for biosynthesis of AgNPs using EFLAE. Presence of SPR signal at 412 nm in curve 3 indicates that 2 hours of time is optimum for biosynthesis of AgNPs using EFLAE.

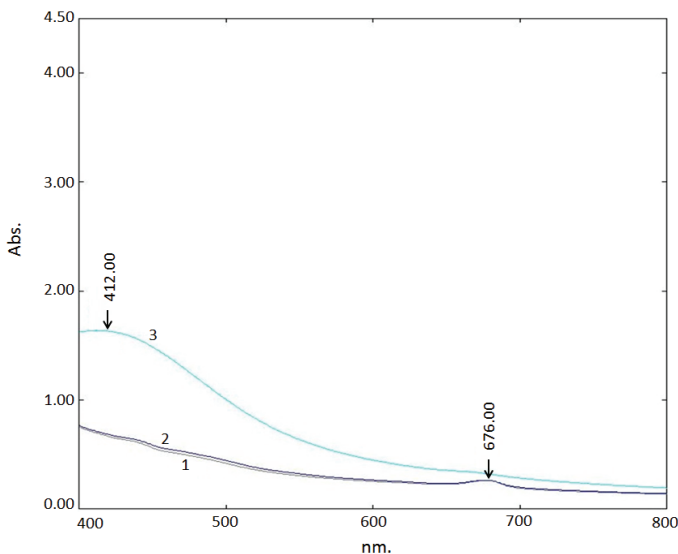


Figure 6: UV-Vis spectrum representing optimization of temperature for green synthesis of AgNPs. Presence of SPR signal at 412 nm in curve 3 indicates that 60°C is optimum for biosynthesis of AgNPs using EFLAE.

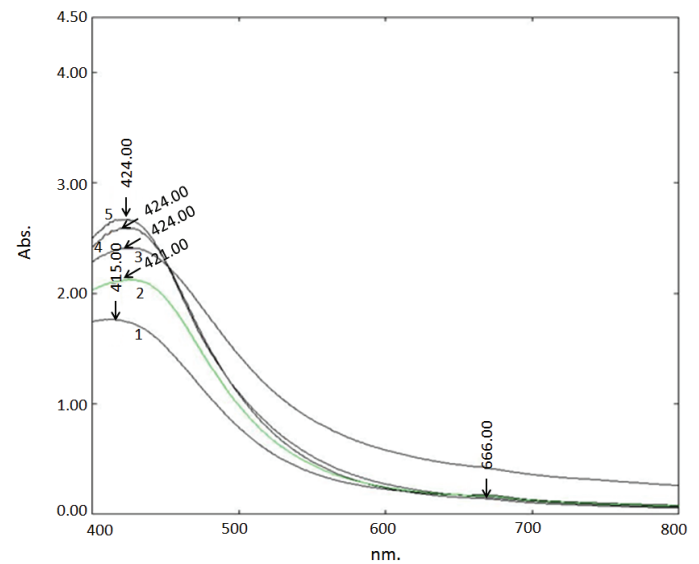


Figure 8: UV-Vis spectrum representing stability of AgNPs. Retention of SPR signal in a range from 412 to 424 nm in all curves indicates that from 2 hours to 30 days, the biosynthesized AgNPs were stable.

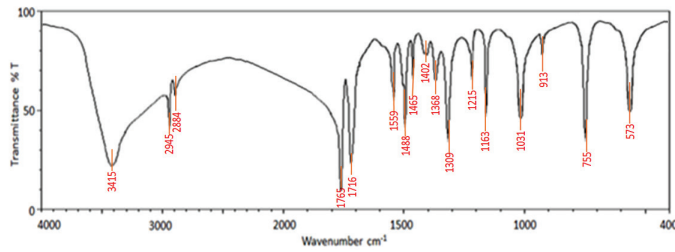


Figure 9: FTIR spectrum represents narrow signals for pure EFLAE.

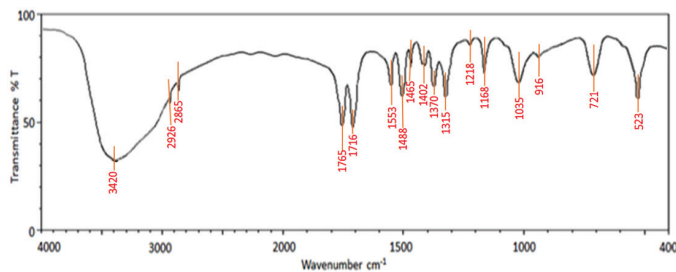


Figure 10: FTIR spectrum represents broadened signals for biogenic AgNPs formed by reduction of Ag⁺ using EFLAE.

E. coli (10 and 18 mm), and *S. pyogenes* (9 and 15 mm) in 50 and 100 µg/ml administered dose. However, pure EFLAE exhibited maximum inhibitory zone against *B. cereus* (7 and 12 mm), followed by *P. aeruginosa* (8 and 14 mm), *E. coli* (6 and 11 mm), and *S. pyogenes* (5 and 9 mm) in 50 and 100 µg/ml administered dose. According to results, the biogenic AgNPs exhibited higher inhibition of against periodontitis causing pathogenic microflora. Results of the present study were also supported by the results of other investigation [19].

4. DISCUSSION

Based on the resultant data, present study confirmed the success of green synthesis of AgNPs from EFLAE. The green synthesis of AgNPs was based on exposure of AgNO₃ to EFLAE. The AgNPs green synthesis reaction progress was monitored for color change and UV-Visible spectrometric analysis. Visual examination of change in color from yellow to brown (Fig. 1) and absorbance signal at 433 nm in the UV-Visible spectrum (Fig. 2) confirmed the formation of AgNPs and reduction of Ag⁺ to Ag⁰. The change in color from yellow to brown and UV-Visible signal at 433 nm together were interpreted as a result of SPR phenomenon (which is a consequence of longitudinal plasmon vibrations stimulation) [47]. There was no possibility of interference of unbound residual biochemical moieties with UV-Visible, FTIR, FESEM, XRD, and EDX data. This is because AgNPs were repeatedly washed and centrifuged using deionized water for removal of any unbound matter.

The UV-Visible spectrometry-based optimization study identified the key parameters for the synthesis of AgNPs using EFLAE, namely: concentration of AgNO₃, volumetric ratio of concentration of EFLAE to AgNO₃, pH, temperature, and time required for green synthesis of AgNPs [44–46]. Optimization of AgNPs biosynthesis based on concentration of AgNO₃ and ratio

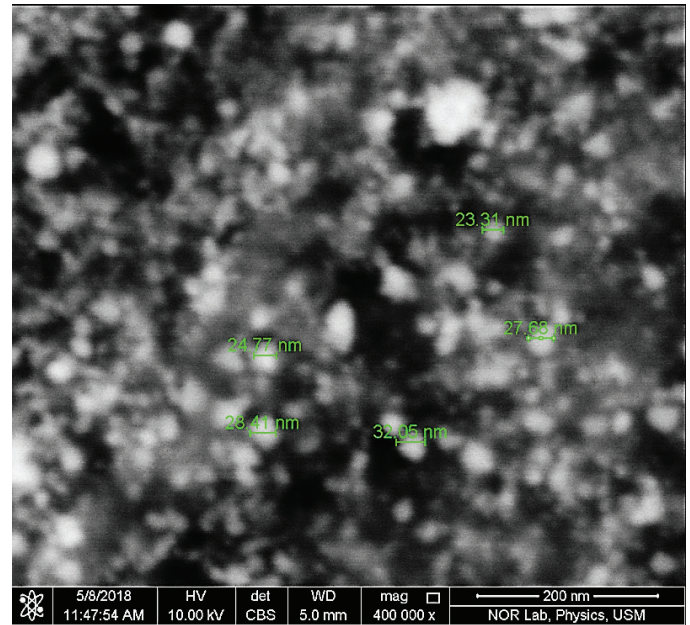


Figure 11: FESEM image represents EFLAE stabilized AgNPs.

of EFLAE to AgNO₃ ratio parameters generated two UV-Visible spectra (Figs. 3 and 4). The spectra given in Figures 3 and 4 represent collective optimization of concentration of AgNO₃, and ratio of EFLAE to AgNO₃. Absence of AgNPs signal in curves 1 and 2 and presence of AgNPs signal at 439 nm in curve 3 reveal that among different volumetric ratio of EFLAE to AgNO₃ and concentrations of AgNO₃, the 1:9 volumetric ratio of EFLAE to AgNO₃ and 5 mM of AgNO₃ concentration were most suitable for AgNPs green synthesis. The optimization results for AgNO₃ concentration (5 mM) and volumetric ratio of AgNO₃ in present study were found in agreement with SPR signal range of other research studies [43,46,47].

The optimization of green synthesis of AgNPs based on different pH (4, 7, and 8) under UV-Visible analysis offered a spectrum given in Figure 5. The Figure 5 illustrates optimization of pH of AgNO₃ and EFLAE solution mixture as parameter. The absence of SPR signal in curves 1 and 3 (related to pH 4 and 8), and retention of SPR signal in curve 2 (related to pH 7) at 426 nm UV-Visible spectrum of Figure 5 supported pH 7 as most suitable pH for production of AgNPs from EFLAE. The results of pH optimization for biosynthesis of AgNPs in present study were verified by observing the similar SPR signal range in other research [46,47].

Optimization of biosynthesis of AgNPs based on different temperatures (8°C–10°C, room temperature, and 60°C) under UV-Visible spectrometer offered a UV-Visible spectrum given in Figure 6. Presence of signal at 412 nm only in curve 3 of Figure 6 revealed that, among three temperatures (8°C–10°C, room temperature, and 60°C), the 60°C temperature is most suitable temperature to synthesize AgNPs from EFLAE. The temperature optimization results over biosynthesis of AgNPs in present study were also supported by other studies with similar SPR signals range [46,47].

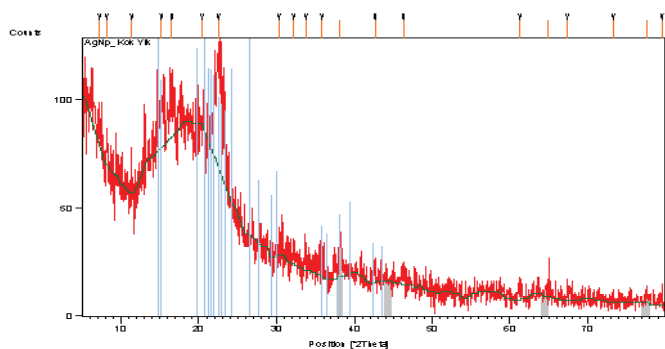


Figure 12: XRD spectrum represents EFLAE stabilized biogenic AgNPs.

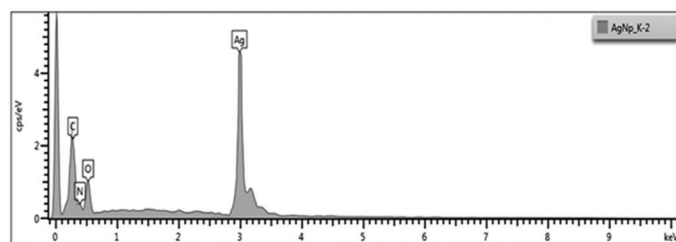


Figure 13: EDX spectrum represents EFLAE stabilized biogenic AgNPs.

Table 1: Antimicrobial activity of EFLAE and AgNPs (Zone of inhibition expressed in mm).

Microorganisms	EFLAE		AgNPs		Ciprofloxacin
	50 µg/ml	100 µg/ml	50 µg/ml	100 µg/ml	
<i>P. aeruginosa</i>	8	14	11	19	22
<i>E. coli</i>	6	11	10	18	20
<i>B. cereus</i>	7	12	13	18	23
<i>S. pyogenes</i>	5	9	9	15	22

The optimization of green synthesis of AgNPs based on different time (½ hour, 1 hour, 2 hours, 4 hours) under UV-Visible spectrometer offered a UV-Visible spectrum given in Figure 7. According to Figure 7, based on the presence of signal at 412 nm, only in curve 3 of Figure 7 revealed that among four time (½ hour, 1 hour, 2 hours, 4 hours), the 2 hours' time is most suitable for biosynthesis of AgNPs from EFLAE. The resultant data of time optimization for AgNPs biosynthesis expressed as SPR signal in present study were supported by other studies also [43,46,47].

The stability of biosynthesized AgNPs was determined using UV-Visible spectrometry (data given in Fig. 8). The synthesized AgNPs were subjected to UV-Vis stability studies after ½ hour, 2 hours, 1 day, 7 days, 15 days, and 30 days (Fig. 8). Figure 8 illustrates increase in absorbance of AgNPs with time. The presence and retention of signals in the range of 415–424 nm supported the stability of AgNPs for 30 days. The stability study result range of AgNPs of present study was in agreement with the other research reports [43,46].

After successful optimization and stability studies, the biosynthesized AgNPs were further subjected to characterization

studies such as FTIR, FESEM, XRD, and EDX analysis to determine the morphology and structure of AgNPs. Prior to characterization studies, the biogenic AgNPs were repeatedly washed and centrifuged using deionized water. This was done to avoid any chance of unbound residual biochemical moieties of EFLAE to interfere with FTIR, FESEM, XRD, and EDX data of AgNPs. The FTIR characterization data indicated formation of AgNPs and the reduction of Ag⁺ to Ag⁰ [46]. Literary evidence supports *E. fusca* to possess flavonoids (5-deoxyglyasperin F and 2'-hydroxyneobavaisoflavanone), alkaloids (erysovine, erythraline, and erysothrine), saponins, and reducing sugars [51]. The signals at 3,415 cm⁻¹ (O-H vibrations), 2,945 and 2,884 cm⁻¹ (C-H vibrations), 1,765 and 1,716 cm⁻¹ (C=O vibrations), 1,559 cm⁻¹ (C=N vibrations), and 1,488 and 1,465 cm⁻¹ (C=C vibrations) also supports to presence of alkaloids and flavonoids in the EFLAE. The FT-IR spectrum of biogenic AgNPs (Fig. 10), when compared with pure FTIR spectrum of EFLAE (Fig. 9), revealed the broadening, marginal shifting, and preservation of FTIR band of AgNPs. For example, narrow signal from 3,415 cm⁻¹ (EFLAE spectrum, Fig. 9) was marginally shifted to broad signal at 3,420 cm⁻¹ (AgNPs spectrum, Fig. 10). Similarly, other signals were also shifted and broadened in AgNPs FTIR spectrum. The shifting and broadening of signals confirm the successful synthesis of biogenic AgNPs. The marginal shift, broadening, and retention of all aforementioned peaks in the FTIR spectrum of AgNPs evidently indicates the dual role of the EFLAE, both as a green reducing agent and capping agent [47]. Based on literary report and FTIR data, it is proposed that alkaloids or flavonoids such as erysovine, erythraline, erysothrine 5-deoxyglyasperin F, and 2'-hydroxyneobavaisoflavanone are key components of EFLAE [51]. These may be responsible for the reduction of silver and resultant biosynthesis of AgNPs as given in Figure 14.

The biogenic AgNPs were subjected to FESEM analysis to establish the size, shape, and distribution of green AgNPs [49,50,52]. The FESEM micrograph given in Figure 11 determined the diverse magnifications and confirmed that biosynthesized AgNPs were well dispersed, spherical in shape, crystalline in nature, smaller than 32 nm in size, and were resulted due to complete reduction of silver from silver nitrate solution by EFLAE.

The XRD spectrometry assisted in determination of crystal nature of biosynthetic AgNPs and was supported by other research evidences [49,50]. The crystalline nature of AgNPs was confirmed by X-ray analysis of XRD pattern (Fig. 12). The analysis of XRD pattern showed the distinctive diffraction peaks at 2θ values of 38.07, 45.22, 64.52, and 78.85 degrees indexed to the 111, 200, 220, and 311 reflection planes of face-centered cubic structure of silver.

To understand the presence of elements contained by AgNPs, the EDX analysis was carried out [50]. The EDX spectrum for AgNPs is given in Figure 13. The resultant data of EDX analysis was found to be comparable with other research also [50,53]. The EDX spectrum showed strong signal in the silver region and confirmed the formation of AgNPs. The spectrum (Fig. 13) revealed silver (84.63%) as a major constituent element compared to carbon (11.48%), oxygen (2.36%), and nitrogen (1.53%). Generally, AgNPs displays typical optical absorption peak at 3 KeV due to SPR [54]. The EDX spectrum exhibited strong signal for silver,

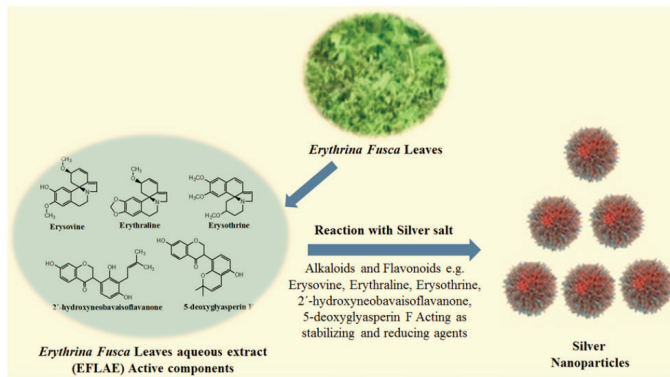


Figure 14: Schematic diagram representing probable mechanism of AgNPs formation using EFLAE. The EFLAE contains several alkaloids and flavonoids such as erysovine, erythraline, erysothrine, 2'-hydroxyneobavaisoflavanone, 5-deoxyglyasperin F, and other constituents. These phytochemicals may reduce the silver salts and stabilize the AgNPs. This figure is adapted from the research work of Nayan et al. [62].

which may be attributed to presence of biochemical moieties that bound on silver surface, resulting in reduction of silver ions to elemental silver. This establishes the ecofriendly reduction of silver compound into AgNPs [55].

Present study involved biogenic AgNPs evaluation for their antimicrobial potential against periodontal disease triggering pathogens of human microbiota, namely: *E. coli*, *P. aeruginosa*, *S. pyogenes*, and *B. cereus*, using well diffusion method. The resultant data of Table 1 revealed that antibacterial activity of green synthesized AgNPs was much higher than EFLAE. The newer AgNPs exhibited maximum zone of inhibition of against *B. cereus* (13 mm at 50 µg/ml and 18 mm at 100 µg/ml) and *P. aeruginosa* (11 mm at 50 µg/ml and 19 mm at 100 µg/ml). The AgNPs displayed significant zone of inhibition against *E. coli* (10 mm at 50 µg/ml and 18 mm at 100 µg/ml) and *S. pyogenes* (9 mm at 50 µg/ml and 15 mm at 100 µg/ml). Compare to AgNPs, the pure EFLAE displayed low zone of inhibition of against *P. aeruginosa* (8 mm at 50 µg/ml and 14 mm at 100 µg/ml) and *B. cereus* (7 mm at 50 µg/ml and 12 mm at 100 µg/ml). The pure EFLAE displayed less zone of inhibition against *S. pyogenes* and *E. coli* (6 mm at 50 µg/ml and 11 mm at 100 µg/ml) and (5 mm at 50 µg/ml and 9 mm at 100 µg/ml). On observation of zone of inhibition of AgNPs, a pattern was observed. That is, an increase in concentration of AgNPs from 50 to 100 µg/ml results in marked increase in zone of inhibition. Several research studies suggested AgNPs extensive application being an antimicrobial and recorded AgNPs higher potential compared to silver ions [56]. The augmentation in antimicrobial response of AgNPs due to biochemical moieties of plant extract (used in biosynthesis of AgNPs) is also mentioned by other studies [47]. The present study antimicrobial results document high potential of AgNPs (biosynthesized using EFLAE) against common opportunistic pathogens of human microbiota. The AgNPs antimicrobial results (biosynthesized using EFLAE) were comparable with ciprofloxacin against common pathogenic gut flora: *E. coli*, *P. aeruginosa*, *S. pyogenes*, and *B. cereus*. The present study results were also supported by other research studies. Many other research studies report that small size and high dose of AgNPs exhibits high antimicrobial response [57–

60]. Therefore, considering the pattern of antimicrobial response exhibited by AgNPs against common opportunistic pathogens of human microbiota in present study, it can be postulated that small size AgNPs (synthesized from EFLAE), when administered in higher dose (100 µg/ml), offer an excellent response against common opportunistic pathogens of gut flora (*E. coli*, *B. cereus*, *S. pyogenes*, and *P. aeruginosa*). The potential of ecofriendly AgNPs of present study to inhibit periodontal disease-causing microorganisms is also supported by other studies, which suggest that plant extract blended AgNPs have potential to inhibit periodontal disease-causing microorganisms [61]. Research evidences accounts *E. fusca* leaves to possess alkaloids, tannins, triterpenoids, glycosides, saponins, and steroids [19]. Hence, as per literary evidences and antimicrobial results of present study, it can be postulated that biochemical moieties of EFLAE (possibly alkaloids and triterpenoids) caused capping of silver and lead to marked increase in antimicrobial potential of AgNPs against periodontitis causing pathogenic microflora. Therefore, based on resultant findings of present study, it is established that AgNPs formulated using EFLAE possess high inhibitory potential against periodontitis triggering pathogens, and recommends EFLAE as potential source for green production of potent AgNPs.

5. CONCLUSION

The UV-Vis, FTIR, FESEM, XRD, and EDX experimental data results of present study supported the success of green synthesis of AgNPs using EFLAE. The synthesis success of biogenic AgNPs was based on physical change in color from yellow to brown and SPR signal at 433 nm. The AgNPs stability, functional group characteristics, and elemental composition were established using UV-Vis, FTIR analysis, and EDX analysis. The morphology of AgNPs was established by FESEM and XRD spectral data. The AgNPs antimicrobial evaluation study against periodontitis causing pathogenic microflora established the excellent inhibition potential of biosynthesized AgNPs against periodontitis triggering pathogens. Hence, based on satisfactory results over green synthesis of AgNPs from EFLAE, optimization, and characterization in present study, the EFLAE is recommended as potential source for green synthesis of highly potent AgNPs. Also, as per inhibitory response exhibited by newer biosynthetic AgNPs against periodontitis triggering bacteria in present study, it is suggested that biogenic AgNPs synthesized using EFLAE exhibiting high inhibitory potential against periodontitis triggering bacteria will be another milestone to heal periodontal disease

ACKNOWLEDGMENTS

Authors are thankful to AIMST University for providing necessary facilities to successfully accomplish this study. Authors are also highly thankful to NanoOptoelectronic Research and Technology (NOR) Lab, School of Physics, University Sains Malaysia for assisting in spectral analysis.

REFERENCES

1. Sender R, Fuchs S, Milo R. Are we really vastly outnumbered? Revisiting the ratio of bacterial to host cells in humans. *Cell* 2016;164:337–40.

2. Sender R, Fuchs S, Milo R. Revised estimates for the number of human and bacteria cells in the body. *PLoS Biol* 2016;14:e1002533.
3. Wang B, Yao M, Lv L, Ling Z, Li L. The human microbiota in health and disease. *Engineering* 2017;3:71–82.
4. Lourenco TGB, Spencer SJ, Alm EJ, Colombo AP. Defining the gut microbiota in individuals with periodontal diseases: an exploratory study. *J Oral Microb* 2018;10:1487741.
5. Tang WW, Kitai T, Hazen SL. Gut microbiota in cardiovascular health and disease. *Cir Res* 2017;120:1183–96.
6. El Kholly K, Genco RJ, Van Dyke TE. Oral infections and cardiovascular disease. *Trends Endocrinol Metab* 2015;26:315–21.
7. Keller A, Rohde JF, Raymond K, Heitmann BL. Association between periodontal disease and overweight and obesity: a systematic review. *J Periodontol* 2015;86:766–76.
8. Borgnakke WS, Yié ostalo PV, Taylor GW, Genco RJ. Effect of periodontal disease on diabetes: systematic review of epidemiologic observational evidence. *J Periodontol* 2013;84:S135–52.
9. Fathi HM, Khairy N, Gheita T, Battawy WAE, Taha R. Clinical significance of periodontitis in rheumatoid arthritis patients: association with disease activity and functional status. *J Arthritis* 2018;7:2.
10. Si Y, Fan H, Song Y, Zhou X, Zhang J, Wang Z. Association between periodontitis and chronic obstructive pulmonary disease in a Chinese population. *J Periodontol* 2012;83:1288–96.
11. Shultis WA, Weil EJ, Looker HC, Curtis JM, Shlossman M, Genco RJ, et al. Effect of periodontitis on overt nephropathy and end-stage renal disease in type 2 diabetes. *Diab Care* 2007;30:306–11.
12. Shillitoe E, Weinstock R, Kim T, Simon H, Planer J, Noonan S, et al. The oral microflora in obesity and type-2 diabetes. *J Oral Microb* 2012;4:19013.
13. Ahn J, Segers S, Hayes RB. Periodontal disease, *Porphyromonas gingivalis* serum antibody levels and orodigestive cancer mortality. *Carcinogen* 2012;33:1055–8.
14. Berezow AB, Darveau RP. Microbial shift and periodontitis. *Periodontol* 2011;55:36–47.
15. Elshagabee FM, Rokana N, Gulhane RD, Sharma C, Panwar H. *Bacillus* as potential probiotics: status, concerns, and future perspectives. *Front Microb* 2017;8:1490.
16. Viciani E, Montagnani F, Tordini G, Romano A, Salemi L, De Luca A, et al. Prevalence of M75 *Streptococcus pyogenes* strains harboring slaA gene in patients affected by pediatric obstructive sleep apnea syndrome in central Italy. *Front Microbiol* 2017;8:294.
17. Culotti A, Packman AI. *Pseudomonas aeruginosa* promotes *Escherichia coli* biofilm formation in nutrient-limited medium. *PLoS One*. 2014;9:e107186.
18. Colombo AP, Magalhaes CB, Hartenbach FA, do Souto RM, da Silva-Boghossian CM. Periodontal-disease-associated biofilm: a reservoir for pathogens of medical importance. *Microb Pathogenesis* 2016;94:27–34.
19. Sudiono J, Sandra F, Halim NS, Kadrianto TA, Melinia M. Bactericidal and cytotoxic effects of *Erythrina fusca* leaves aquadest extract. *Dent J Majal Kedokt Gigi* 2013;46:9–13.
20. Patra JK, Baek K-H. Antibacterial activity and synergistic antibacterial potential of biosynthesized silver nanoparticles against foodborne pathogenic bacteria along with its anticandidal and antioxidant effects. *Front Microbiol* 2017;8:167.
21. Yuan Y-G, Peng Q-L, Gurunathan S. Effects of silver nanoparticles on multiple drug-resistant strains of *Staphylococcus aureus* and *Pseudomonas aeruginosa* from mastitis-infected goats: an alternative approach for antimicrobial therapy. *Int J Mol Sci* 2017;18:569.
22. Barros C, Fulaz S, Stanisic D, Tasic L. Biogenic nanosilver against multidrug-resistant bacteria (MDRB). *Antibiotics* 2018;7:69.
23. Goudarzi M, Mir N, Mousavi-Kamazani M, Bagheri S, Salavati-Niasari M. Biosynthesis and characterization of silver nanoparticles prepared from two novel natural precursors by facile thermal decomposition methods. *Sci Rep* 2016;6:32539.
24. Jain S, Mehata MS. Medicinal plant leaf extract and pure flavonoid mediated green synthesis of silver nanoparticles and their enhanced antibacterial property. *Sci Rep* 2017;7:15867.
25. Cohen-Karni T, Langer R, Kohane DS. The smartest materials: the future of nanoelectronics in medicine. *ACS Nano* 2012;6:6541–5.
26. Escarcega-Gonzalez CE, Garza-Cervantes J, Vazquez-Rodríguez A, Montelongo-Peralta LZ, Treviño-González MT, Castro ED, et al. In vivo antimicrobial activity of silver nanoparticles produced via a green chemistry synthesis using *Acacia rigidula* as a reducing and capping agent. *Int J Nanomed* 2018;13:2349.
27. Mohammed AE, Al-Qahtani A, Al-Mutairi A, Al-Shamri B, Aabed K. Antibacterial and cytotoxic potential of biosynthesized silver nanoparticles by some plant extracts. *Nanomater* 2018;8:382.
28. Loo YY, Rukayadi Y, Nor-Khaizura MA, Kuan CH, Chieng BW, Nishibuchi M, et al. In vitro antimicrobial activity of green synthesized silver nanoparticles against selected gram-negative foodborne pathogens. *Front Microbiol* 2018;9:1555.
29. Venkatesan J, Singh SK, Anil S, Kim S-K, Shim MS. Preparation, characterization and biological applications of biosynthesized silver nanoparticles with chitosan-fucoidan coating. *Molecules* 2018;23:1429.
30. Rai M, Deshmukh S, Ingle A, Gade A. Silver nanoparticles: the powerful nanoweapon against multidrug-resistant bacteria. *J Appl Microbiol* 2012;112:841–52.
31. Abdelmoteleb A, Valdez-Salas B, Cecena-Duran C, Tzintzun-Camacho O, Gutiérrez-Miceli F, Grimaldo-Juarez O, et al. Silver nanoparticles from *Prosopis glandulosa* and their potential application as biocontrol of *Acinetobacter calcoaceticus* and *Bacillus cereus*. *Chem Spec Bioavail* 2017;29:1–5.
32. Francis S, Joseph S, Koshy EP, Mathew B. Microwave assisted green synthesis of silver nanoparticles using leaf extract of *Elephantopus scaber* and its environmental and biological applications. *Artif Cells Nanomed Biotech* 2018;46:795–804.
33. Abbasi E, Milani M, Fekri Aval S, Kouhi M, Akbarzadeh A, Tayefi Nasrabadi H, et al. Silver nanoparticles: synthesis methods, bio-applications and properties. *Crit Rev Microbiol* 2016;42:173–80.
34. Suriati G, Mariatti M, Azizan A. Synthesis of silver nanoparticles by chemical reduction method: Effect of reducing agent and surfactant concentration. *Int J Autom Mech Eng* 2014;10:1920.
35. Nasretidinova G, Fazleeva R, Osin YN, Gubaidullin AT, Yanilkin VV. Methylviologen-mediated electrochemical synthesis of silver nanoparticles via the reduction of AgCl nanospheres stabilized by cetyltrimethylammonium chloride. *Rus J Electrochem* 2017;53:25–38.
36. Mehmood A, Murtaza G, Bhatti TM, Kausar R. Enviro-friendly synthesis of silver nanoparticles using *Berberis lycium* leaf extract and their antibacterial efficacy. *Acta Metall Sin (Eng Lett)* 2014;27:75–80.
37. Gomathi M, Rajkumar P, Prakasam A, Ravichandran K. Green synthesis of silver nanoparticles using *Datura stramonium* leaf extract and assessment of their antibacterial activity. *Res Eff Tech* 2017;3:280–4.
38. Mittal J, Jain R, Sharma MM. Phytofabrication of silver nanoparticles using aqueous leaf extract of *Xanthium strumarium* L. and their bactericidal efficacy. *Adv Nat Sci Nanosci Nanotech* 2017;8:025011.
39. Li F, Hullar MA, Schwarz Y, Lampe JW. Human gut bacterial communities are altered by addition of cruciferous vegetables to a controlled fruit-and vegetable-free diet. *J Nutr* 2009;139:1685–91.
40. Shittu K, Ihebunna O. Purification of simulated waste water using green synthesized silver nanoparticles of *Piliostigma thonningii* aqueous leaf extract. *Adv Nat Sci Nanosci Nanotech* 2017;8(4):045003.
41. Ravichandran V, Vasanthi S, Shalini S, Shah SA, Harish R. Green synthesis of silver nanoparticles using *Atrocarpus altilis* leaf extract and the study of their antimicrobial and antioxidant activity. *Mat Lett* 2016;180:264–7.
42. Wang C, Mathiyalagan R, Kim YJ, Castro-Aceituno V, Singh P, Ahn S, et al. Rapid green synthesis of silver and gold nanoparticles using

- Dendropanax moribifera* leaf extract and their anticancer activities. Int J Nanomed 2016;11:3691.
43. Veerasamy R, Xin TZ, Gunasagaran S, Xiang TF, Yang EF, Jeyakumar N, et al. Biosynthesis of silver nanoparticles using mangosteen leaf extract and evaluation of their antimicrobial activities. J Saudi Chem Soc 2011;15:113-120.
 44. Ovais M, Khalil AT, Raza A, Khan MA, Ahmad I, Islam NU, et al. Green synthesis of silver nanoparticles via plant extracts: beginning a new era in cancer theranostics. Nanomed 2016;12:3157-77.
 45. Saxena J, Sharma PK, Sharma MM, Singh A. Process optimization for green synthesis of silver nanoparticles by *Sclerotinia sclerotiorum* MTCC 8785 and evaluation of its antibacterial properties. SpringerPlus 2016;5:861.
 46. Erjaee H, Rajaian H, Nazifi S. Synthesis and characterization of novel silver nanoparticles using *Chamaemelum nobile* extract for antibacterial application. Adv Nat Sci Nanosci and Nanotech 2017;8:025004.
 47. Shaik MR, Khan M, Kuniyil M, Al-Warthan A, Alkhatlan H, Siddiqui M, et al. Plant-extract-assisted green synthesis of silver nanoparticles using *Origanum vulgare* l. extract and their microbicidal activities. Sustainability 2018;10:913.
 48. Logeswari P, Silambarasan S, Abraham J. Ecofriendly synthesis of silver nanoparticles from commercially available plant powders and their antibacterial properties. Sci Iran 2013;20:1049-54.
 49. Anandalakshmi K, Venugobal J, Ramasamy V. Characterization of silver nanoparticles by green synthesis method using *Petalium murex* leaf extract and their antibacterial activity. Appl Nanosci 2016;6:399-408.
 50. Banala RR, Nagati VB, Karnati PR. Green synthesis and characterization of *Carica papaya* leaf extract coated silver nanoparticles through X-ray diffraction, electron microscopy and evaluation of bactericidal properties. Saudi J Biol Sci 2015;22:637-44.
 51. Suley PR, Gonzalez-Guevara JL, García-Torres M, Carballo-González MT, Echemendia-Arana OA, Garrido-Garrido G, et al. Preliminary phytochemical screening and in vitro antiherpetic activity of *Erythrina fusca* Lour. Acta Farm Bonaerense 2004;23:453-8.
 52. Deljou A, Goudarzi S. Green extracellular synthesis of the silver nanoparticles using *Thermophilic Bacillus* sp. AZ1 and its antimicrobial activity against several human pathogenetic bacteria. Iran J Biotech 2016;14:25.
 53. Ashraf JM, Ansari MA, Khan HM, Alzohairy MA, Choi I. Green synthesis of silver nanoparticles and characterization of their inhibitory effects on AGEs formation using biophysical techniques. Sci Rep 2016;6:20414.
 54. Dakhil AS. Biosynthesis of silver nanoparticle (AgNPs) using *Lactobacillus* and their effects on oxidative stress biomarkers in rats. J King Saud Univ Sci 2017;29:462-7.
 55. Jyoti K, Baunthiyal M, Singh A. Characterization of silver nanoparticles synthesized using *Urtica dioica* Linn. leaves and their synergistic effects with antibiotics. J Rad Res Appl Sci 2016;9:217-27.
 56. Yan X, He B, Liu L, Qu G, Shi J, Hu L, et al. Antibacterial mechanism of silver nanoparticles in *Pseudomonas aeruginosa*: proteomics approach. Metallomics 2018;10:557-64.
 57. Dakal TC, Kumar A, Majumdar RS, Yadav V. Mechanistic basis of antimicrobial actions of silver nanoparticles. Front Microbiol 2016;7:1831.
 58. Kim DH, Park JC, Jeon GE, Kim CS, Seo JH. Effect of the size and shape of silver nanoparticles on bacterial growth and metabolism by monitoring optical density and fluorescence intensity. Biotech Bioeng 2017;22:210-7.
 59. Gurunathan S, Choi YJ, Kim JH. Antibacterial efficacy of silver nanoparticles on endometritis caused by *Prevotella melaninogenica* and *Arcanobacterium pyogenes* in dairy cattle. Int J Mol Sci 2018;19:1210.
 60. Pazos-Ortiz E, Roque-Ruiz JH, Hinojos-Márquez EA, López-Esparza J, Donohué-Cornejo A, Cuevas-González JC, et al. Dose-dependent antimicrobial activity of silver nanoparticles on polycaprolactone fibers against gram-positive and gram-negative bacteria. J Nanomat 2017;2017:1-7.
 61. Emmanuel R, Palanisamy S, Chen SM, Chelladurai K, Padmavathy S, Saravanan M, et al. Antimicrobial efficacy of green synthesized drug blended silver nanoparticles against dental caries and periodontal disease causing microorganisms. Mat Sci Eng C 2015;56:374-9.
 62. Nayan V, Onteru SK, Singh D. *Mangifera indica* flower extract mediated biogenic green gold nanoparticles: Efficient nanocatalyst for reduction of 4-nitrophenol. Environ Prog Sustain Energy 2018;37:283-94.

How to cite this article:

Fuloria NK, Fuloria S, Chia KY, Karupiah S, Sathasivam K. Response of green synthesized drug blended silver nanoparticles against periodontal disease triggering pathogenic microbiota. J Appl Biol Biotech 2019;7(04): 46-56. DOI: 10.7324/JABB.2019.70408